ESPACE

Receiver Technology

Signal acquisition and processing

Hrishik Mishra
3rd semester

I. Abstract

Before the navigation solution for the receiver position using Global Positioning Satellite (GPS) signals is obtained, the signal passes through the antenna, the front-end, baseband signal processing (Acquisition and Tracking). The latter two are employed in multi-channel hardware while the navigation solution itself is merely a software solution. In the following report, the basic design aspects of a GPS-receiver's baseband signal processing is discussed. The acquisition process is simulated using MATLAB code and, by using downsampled digital receiver signals as well as generated GPS signals, the signal processing is examined. Among all, the conventional Time-Frequency-Space-Search and the Parallel-Time-Space-Search (FFT-IFFT) methods are investigated for acquisition. For this purpose, the Coarse Acquisition (CA) code is generated and correlation outputs are examined. The correlation principle is used for identifying the satellites from which measurements can be extracted. In reality, however, if a receiver has been operational, it may employ the GPS almanac message in its memory to fasten the process. Among the first unknowns in signal processing are code delay and Doppler shift (due to relative motion between transmitter and receiver). After having resolved this in the acquisition process, the tracking loops ensure that the internal replica of the receiver is best aligned with the incoming GPS signal in terms of code delay, Doppler frequencies and carrier phase. Usually, the code tracking is implemented using Delay locked loops (DLL) while the carrier phase tracking can be employed using either Phase locked loops (PLL) or Frequency locked loops (FLL). In the following report, the DLL and PLL have been examined.

II. Implementing a Sampled C/A code generator with code delay

The GPS-satellites make use of Direct Sequence Spread Spectrum (DSSS) to spread the navigation data by using a pseudo-random sequence (PRN) which runs at a faster rate (chipping) and modulates the navigation data. For multiple access, the GPS-satellites employ Code Division Multiple Access (CDMA). PRN codes achieve both of these functionalities with limited hardware requirements (Linear Feedback Shift Registers, LFSR). Since the Chipping time T_c of the PRN is more than the navigation message pulse duration T_d itself, the bandwidth of the spread spectrum is much higher than the original signal. The ratio of T_d and T_c is called spreading factor.

PRN code has a spread spectrum similar to random bit-sequence but is deterministically generated. Most commonly used DSSS codes are Maximum Length Sequences (MLS) which are periodic with $2^N - 1$. The GPS signals use Gold codes which are generated with Modulo-2 addition (XOR) operations. The PRN codes have a desirable property in autocorrelation that it is high while the crosscorrelation outputs are low. Every satellite comprises of two shift registers, $G1$and $G2$, which generate a MLS of 1023 bits. The chipping rate is 1.023 MHz. And hence, the repletion time for a PRN code sequence is, very simply, nearly 1ms. An example of the generation process is demonstrated in Figure 1. The $G1$ LFSR has XOR operation between 3 and 10 (Polynomial: $1 + x^3 + x^{10}$ for PRN:1. The $G2$ feedback is a XOR operation on outputs from positions: 2, 3, 6, 8, 9 and 10 (Polynomial: $1 + x^2 + x^3 + x^6 + x^8 + x^9 + x^{10}$). The outputs from G1 and G2 are taken according to GPS specification and operated again with XOR operation to obtain the C/A code for a given satellite.

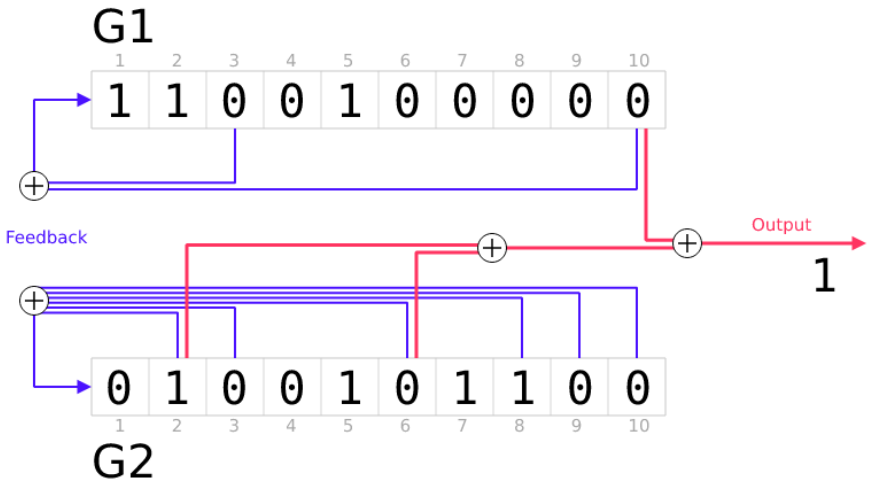

Figure 1. Implementation of PRN:1 code using Shift registers.

The CA code for PRN:1 was generated and verified by finding the octal equivalent of the 10 code chips and matching with the GPS specification. For the given example of PRN:1, the octal equivalent was found to be 1440. A 1ms CA code is demonstrated in Figure 2.

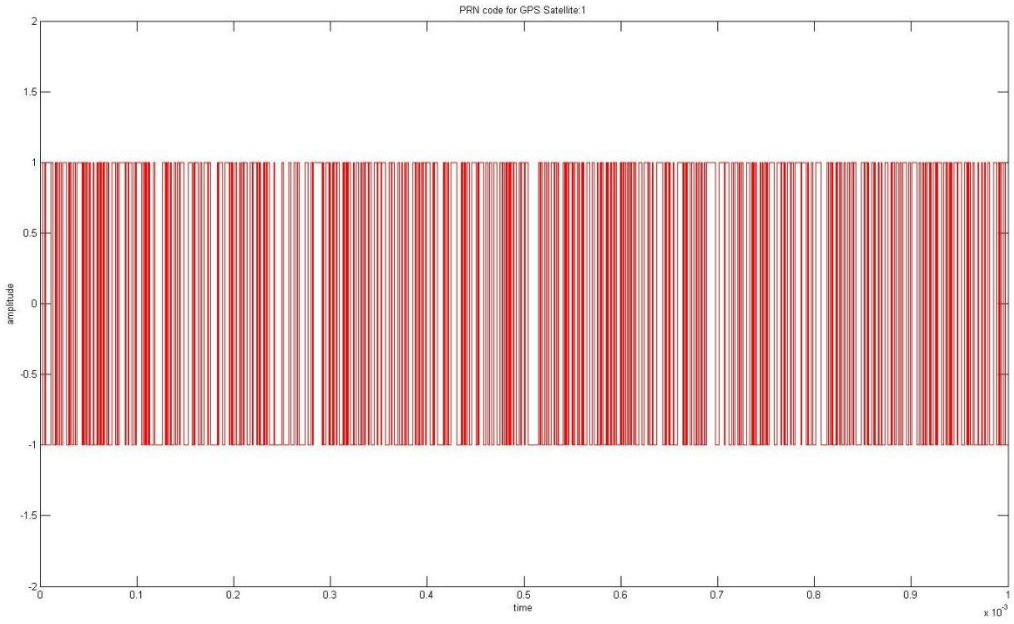

Figure 2. CA code for PRN:1 (octal equivalent of 10 chips = 1440)

The autocorrelation property of the generated CA code was verified and the normalized correlation values are found to be [-0.065, -0.001, 0.063, 1]. The results are show in Figure 3.

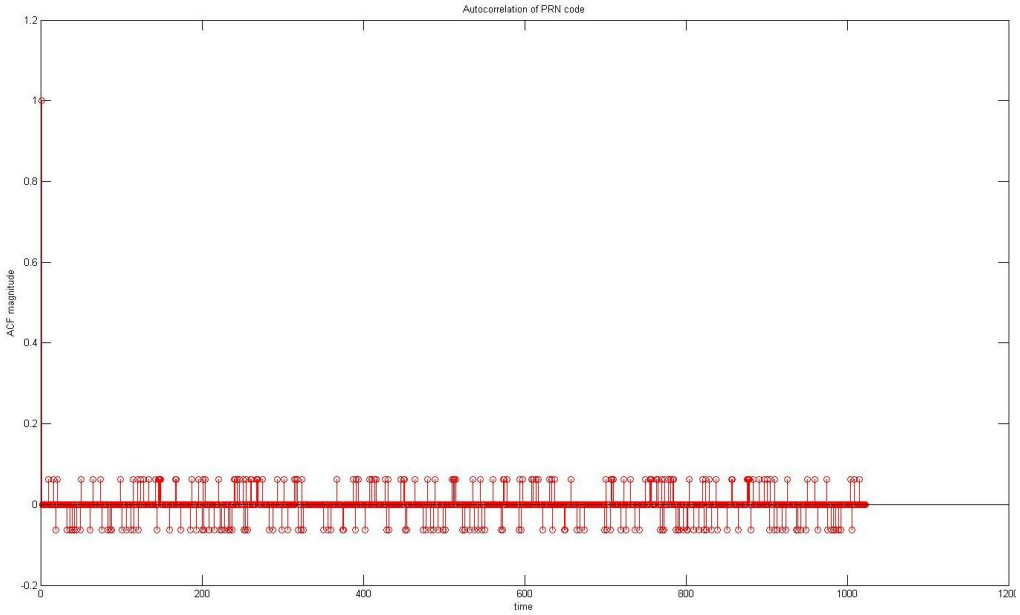

Figure 3. Autocorrelation function for PRN:1 CA code

The crosscorrelation results also yield the values in the same bounded values, [-0.065, -0.001, 0.063]. But, it can be seen that there is no correlation between the signals. In the following example PRN:1 and PRN:2 have been used as signal generators. In Figure 4, it can be verified that the

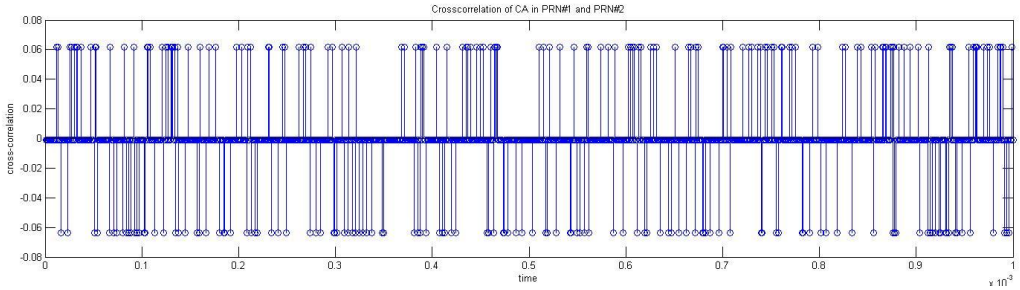

Figure 4. Crosscorrelation function between CA code of PRN:1 and PRN:2

The autocorrelation and cross-correlation results for the sampled CA code are shown in Figure 5. As expected, they follow the patterns as in the case of unsampled code.

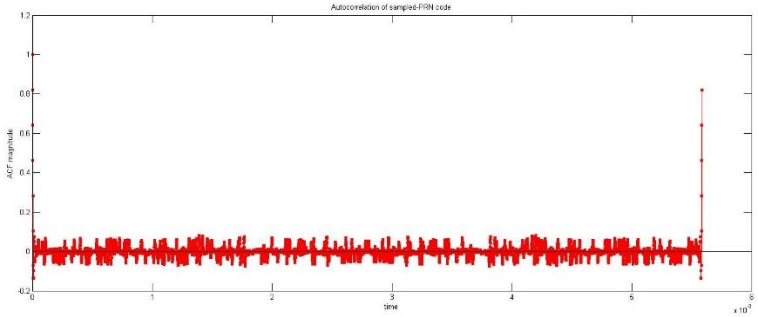

Figure 5. Autocorrelation function of sampled CA code of PRN:1

The result is still showing a maximum correlation around zero lag of the autocorrelation function. However, due to the circular correlation, there is a significant function value at lags close to the end of sampling period. However, this only emphasizes the correlation peak close to zero lag.

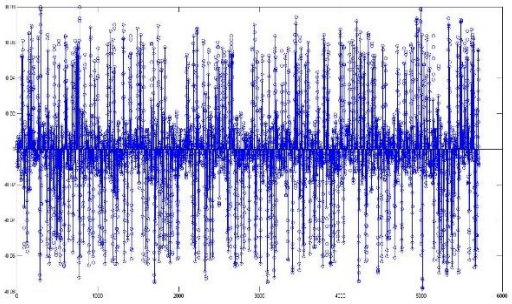

Figure 6. Crosscorrelation function between sampled CA code of PRN:1 and PRN:2

Figure 6 reiterates the fact that the cross-correlation between two different PRN-sequences have low correlation values.

In figure 7, the details of the recorded Intermediate Frequency signal (IF) for a length of 0.001 seconds has been shown. The time-series is clipped between [-3,3] which suggests a 4-bit quantization of the GPS receiver. And the Periodogram analysis emphasizes that the signal has a peak at the L1-carrier frequency ($154 \times 10.23 \times 10^6\ Hz$). But due to the DSSS, as mentioned above, the signal is spread over the frequency domain like white noise.

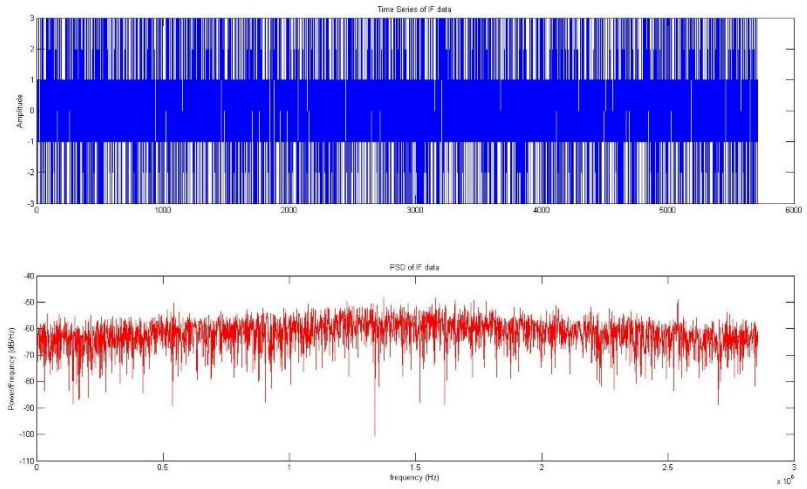

Figure 7. Intermediate Frequency (IF) signal details ($1ms$) a)time-series b)Periodogram

III. Signal Acquisition

Acquisition is the signal processing in the baseband processing module of GPS receivers which concerns with a three-dimensional search in time (code phase), frequency (Doppler shift) and satellite-specific PRN code. For a receiver, that is able to read the GPS-almanac data from its memory, the visible satellites can usually be predicted in advance. As a result, the search reduces to a two-dimensional space for code phase and frequency. The signal being received at the GPS antenna of the receiver is affected by the relative motion between the satellite and the receiver. For terrestrial measurements, the major contribution to Doppler shift in carrier frequency is the GPS satellite's motion in the radial direction. For a static receiver, the variation can be as big as $\pm 5\ KHz$. The main purpose of signal acquisition is to find a coarse estimation of this frequency shift along with the code-phase in the signal that has been captured. The minimum signal length for this purpose is $1ms$, which is the length of CA code.

The simplest implementation of acquisition is the conventional serial search in the Code time-phase and Frequency space. In the following exercise, a non-coherent implementation is employed under the assumption that the code-phase received is purely random.

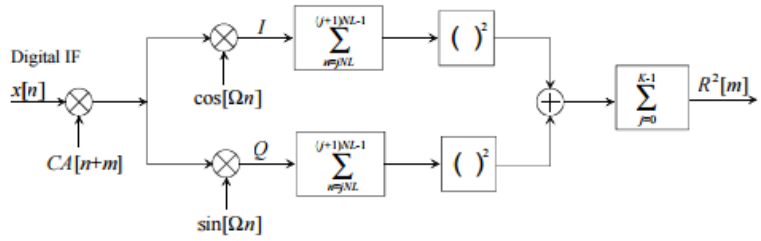

Figure 8. Serial Code time-phase Frequency search block diagram

Firstly, the digital IF signal, $x[n]$ is multiplied with the locally generated CA code. After this code-removal, the In-phase (I) and the quadrature (Q) components are generated by using apt carrier waves. The I and Q components are accumulated over N (1, in this case) periods. The accumulated sum, therefore gives us the correlation coefficient for the given code-phase and frequency.

$$R^2[m] = \sum \left(\left[\sum x[n].CA[n] \cos[\Omega n] \right]^2 + \left[\sum x[n].CA[n] \sin[\Omega n] \right]^2 \right) \qquad \text{(i)}$$

Equation i. gives us mathematical equivalent of the correlation coefficient being computed for each code-phase and frequency. In the given exercise, for PRN:4, the following correlation mountain figure was obtained as shown in figure 9.

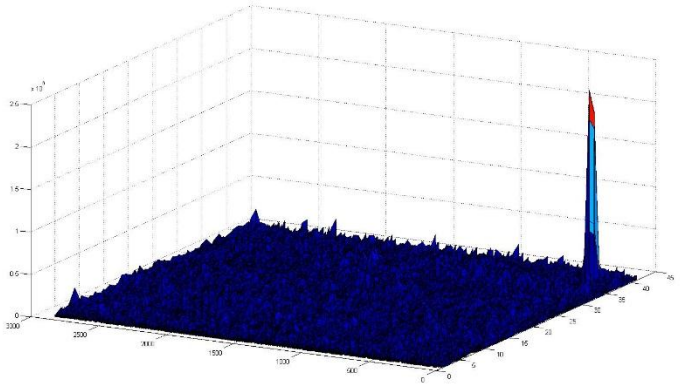

Figure 9. Correlation mountain for PRN:4 using Serial search technique

Table:1, PRN:4 acquisition	
Code phase	61.5877 chips
Frequency shift	7500 Hz

With a Frequency-bin of 500 Hz and a code-phase of 0.3581, the following parameters in Table:1, were obtained.

Since, the acquisition is a coarse estimate of the Doppler Frequency shift, a Frequency-bin of 500 Hz was used instead of the suggested 250 Hz for faster processing in case of the conventional search.

A much faster implementation of the two-dimensional search space is the Parallel-code phase search (FFT-IFFT) method. The main requirements of acquisition phase is the sensitivity of acquisition and the acquisition time itself. In order to fasten the process, the computational ease of the FFT-algorithm is employed. As shown in Figure 10, the block diagram of the FFT-IFFT method makes use of the property that "correlation in the time-domain is a multiplication in the frequency-domain".

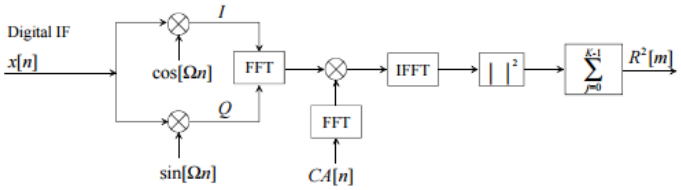

Figure 10. Parallel-code search technique block diagram

Equation ii. provides the mathematical basis for the FFT-IFFT method.

$$R[m] = x[n] * CA[-n] = \mathcal{F}^{-1}[\mathcal{F}(x[n]).\mathcal{F}(CA[n])^*] \quad \text{(ii)}$$

In the following approach, the incoming IF signal is mixed to the baseband signal and the I and Q components are then directly correlated with the CA code replica that is generated using FFT-algorithms. The resultant correlation coefficients are then computed iteratively for each Frequency bin.

By employing the FFT-IFFT algorithm, the following satellites were obtained with a strong enough signal.

Table:2		
PRN	**Code phase [samples]**	**Doppler Frequency [Hz]**
1	4806	-10000
4	342	-8500
7	2211	-7000
13	1938	-4000
24	3746	1500

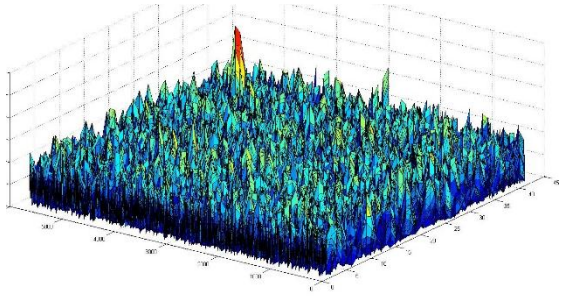

Figure 11. Correlation mountain for PRN:1

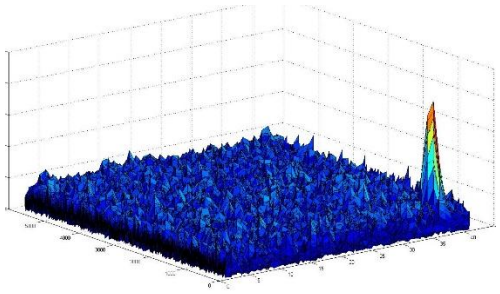

Figure 12. Correlation mountain for PRN:4

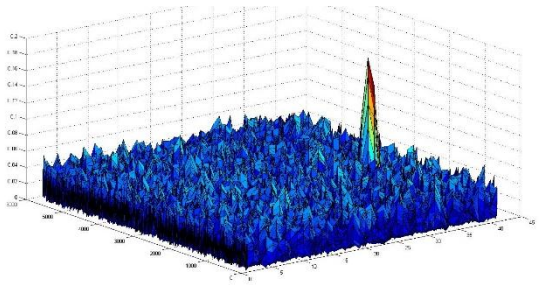

Figure 13. Correlation mountain for PRN:7

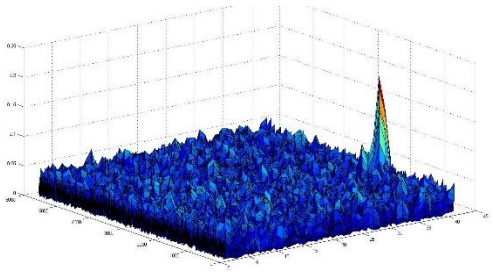

Figure 14. Correlation mountain for PRN:13

Figures 11-14 summarize the Correlation Mountains for PRNs [1, 4, 7, and 13]. Based on the Threshold criteria, only these 5 satellites were considered valid for the next step of tracking. The total search space for the FFT-IFFT method was 5714×41. However, because of faster resolution of FFT-algorithms in MATLAB, the total search time was drastically reduced. And, this is the more efficient method to implement an acquisition software.

IV. Signal Generator implementation

As a part of the exercise, a signal generator was implemented which simulates the Front-end section of the typical GPS-receiver. After the signal is received at the antenna, the signal is converted to an Intermediate Frequency (IF) through mixing and then sampled (downsampling). The signal generator simulates the generation of the IF signal by replicating the PRN-code generation and mixing with the carrier wave. A white-noise generator is used to infect the ideal IF signal with noise.

Equation (iii) refers to the signal model that is received after downsampling.

$$s(t_k) = \sqrt{2.P}.D(t_k - \tau).CA(t_k - \tau).\cos(2\pi(f_{IF} + f_D)t_k + \varphi_0) + \epsilon_{N(\mu,\sigma^2)} \quad \text{(iii)}$$

Where,

$f_{IF} = 4.3\ MHz$: Intermediate Frequency

$f_D = 3 \times 10^3 Hz$: Doppler Frequency

φ_0: Initial Carrier phase

τ: Code phase delay

CA: CA code sequence (PRN-code)

D: Navigation data bit

$P = -158.5\ dB$: Received Power

$\epsilon_{N(\mu,\sigma^2)}$: $Additive\ White\ Gaussian\ Noise$

For the sampling period of T_s = 1/5.714x106 sec, 5714 samples of both Carrier and PRN-code were generated for creating a total signal length of $1ms$. The given data was used to simulate an IF signal that could be used for further analysis.

$$\sigma_{noise} = \sqrt{f_{IF}.P_{received} \Big/ \left(\frac{C}{N_0}\right)} \quad \text{(iv)}$$

Equation (iv) was used to convert the typical $\frac{C}{N_0}$ values to the variance of additive noise.

The generated signal was then tested for Acquisition again and the correlation mountain is shown in figure 15. The correlation details are shown in Table:3.

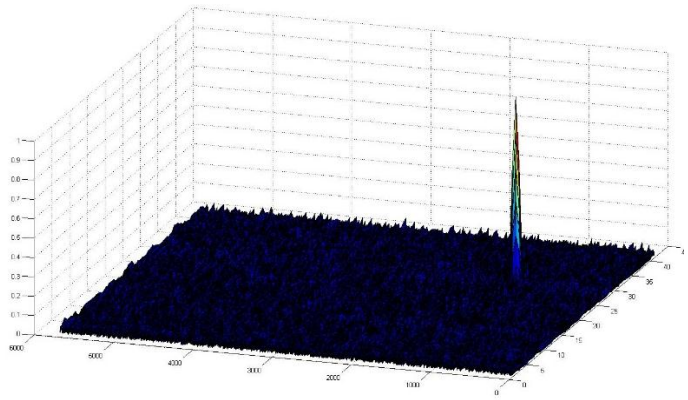

Figure 15. Correlation mountain for PRN:1 using Signal generator

Table:3, PRN:1 acquisition	
Code phase	1125 samples
Frequency shift	3000 Hz

Based on the results, it can be validated that the signal generator is providing an appropriate IF signal for simulation purposes.

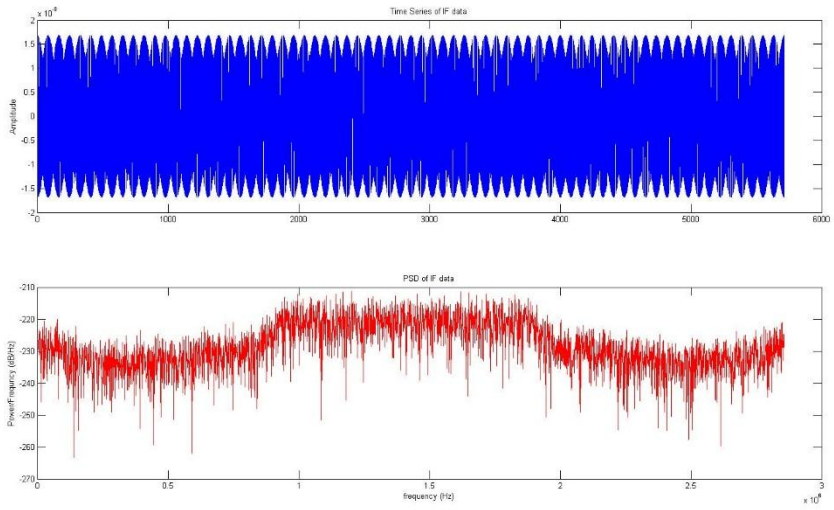

Figure 16. Time-series and Frequency-domain representation of generated signal (1ms)

V. Acquisition time-analysis on GALILEO signals

	GPS	**GALILEO**
Option	L1-C/A	OS-E1
Code rate [Mcps]	1.023	1.023
Code length [chips]	1023	4092
Code duration [ms]	1	4
Data rate [sps]	50	250
Required $\frac{C}{N_0}$	40	35
Size of Search space ($\Delta T \times \Delta f$)	$[1023 \times 2.5K]$	$[4092 \times 2.5K]$
Size of Search grid $\delta T \times \delta f$)	$[0.5 \times 660]$	$[0.5 \times 660]$
T_{acq} for one SV [s]	32	32

Typically, a code bin of 0.5 chips is used for accuracy purposes whereas a Doppler bin of 660 Hz ($\frac{2.T}{3}$) is used to obtain merely a coarse Frequency estimate.

One of the modernization in GPS signals and the Galileo signals is the introduction of the binary offset carrier (BOC) modulation. BOC modulations offer sub-carrier frequency f_s in MHz and spreading code rate f_c in Mcps (Mega Chips Per Second). These two parameters provide freedom to concentrate signal power within specific parts of the allocated band to reduce interference with the reception of other signals. So by concentrating power on some particular area, helps in side lobes suppression. In the acquisition stage, if a high code-bin is used, it is possible that the main correlation peak cannot be detected. The acquisition samples are the result of correlation. As discussed in previous chapters that decision is made with respect to these correlation samples. The step between two successive uncertain delays is expressed in code chips. As can be observed in the figure 17, that the maximum peak can be missed if a code chip of size 0.5 chip will be used, which will cause a fatal effect on the whole acquisition process. One possibility to make the correlation main peak detectable is shrink the code bin but that will charge a larger acquisition time, since more time bins need to be scanned. Other possibility is to refine the ambiguous correlation into an unambiguous, via frequency-domain or time-domain processing. In general, it can be concluded that the GALILEO signal is not as effective as GPS when it comes to the acquisition process.

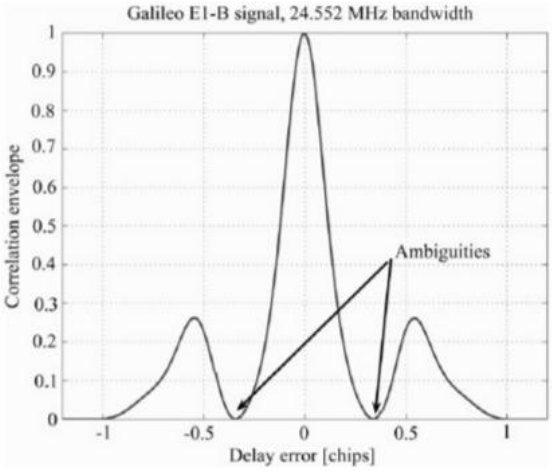

Figure 17. Ambiguities in BOC modulated signal with 24.552 MHz double-sided front-end bandwidth

VI. Signal Tracking

Once the Acquisition phase is over and the "visible" satellites have been determined along with coarse predictions of code phase and frequency shift, the signal has to be tracked with preciseness for the navigation data to be appropriately generated. For this purpose, the tracking loops ensure that the code phase, the initial carrier phase and the frequency shifts are tracked within tolerance limits. A control loop tracks these parameters and controls the output of the prompt replicated signal in the GPS receiver. A general block diagram of the tracking loop is show in Figure 18.

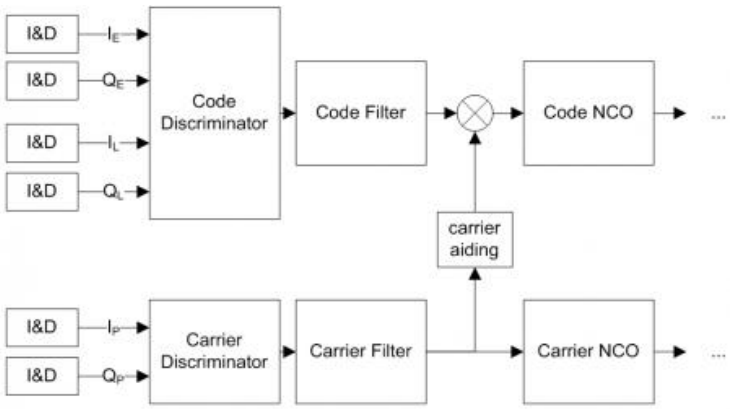

Figure 18. Ambiguities in BOC modulated signal with 24.552 MHz double-sided front-end bandwidth

While the code phase is tracked by using a Delay Locked Loop (DLL), the carrier phase is tracked using either a Phase Locked Loop (PLL) with respect to carrier phase itself or the Doppler frequency using a Frequency Locked Loop (FLL).

The Delay Locked Loop is a combination of Integrate-and-Dump (ID), filter and Numerically Controlled Oscillator (NCO) which produces the correction in Code Phase which is then used to control the NCO output for the CA code. In addition to the Prompt (in-phase) correlation, it produces an Early and a Late correlation too which are separated by one code chip. This enables the receiver to determine the direction of the change in Code Phase and the magnitude. The difference between the Early and Late correlators produces the S-curve. Tracking of the zero-crossing of the S-curve is used to estimate the error.

$$I_E = AdR_x\left(\tau_e - \frac{\delta}{2}\right)\cos(\varphi_e) \quad \text{(v)}$$

$$Q_E = -AdR_x\left(\tau_e - \frac{\delta}{2}\right)\sin(\varphi_e) \quad \text{(vi)}$$

$$I_L = AdR_x\left(\tau_e + \frac{\delta}{2}\right)\cos(\varphi_e) \quad \text{(vii)}$$

$$Q_L = -AdR_x\left(\tau_e + \frac{\delta}{2}\right)\sin(\varphi_e) \quad \text{(viii)}$$

Where,

τ_e: Code delay error estimated by receiver

φ_e: Carrier phase error estimated by receiver

δ: Early-Late spacing (1-chip)

A: Amplitude

d: Navigation data

R_x: Autocorrelation function of PRN code

In the following exercise, the specifications were used to generate the test GPS signal using the signal generator. The Early-Late and Prompt replicas were created to simulate the DLL. The responses can be verified in Figure 19.

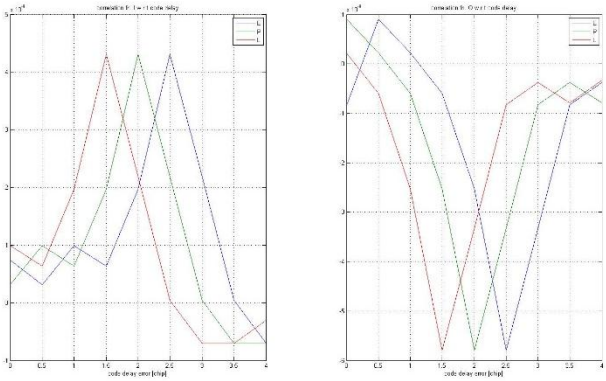

Figure 19. Correlation peaks for Early, Late and Prompt replicas for I and Q components with respect to code phase.

The correlation coefficients for Early and Late correlators is exactly half the Prompt value at tracked code phase value (0 in this case). In Figure 20, it can be verified that the correlations of E-P-L arms are at the same Doppler Frequency (0 as specified). However, the magnitudes for E-L arms are significantly reduced for the given Code-Phase (0).

Similarly, in Figure 21, an initial carrier phase of angle of 90 degrees results in the correlation peaks for I and Q components. And as in the previous case, the correlation peaks for E-L arms are much reduced as compared to the P arm.

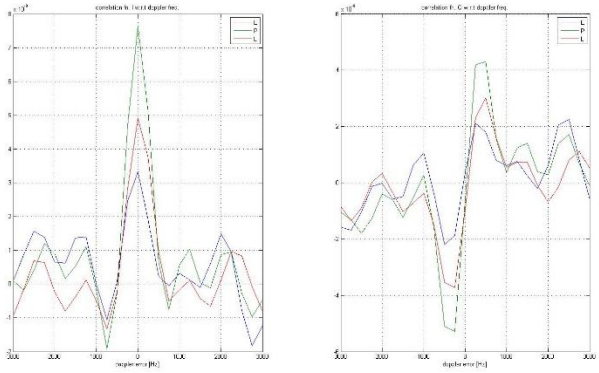

Figure 20. Correlation peaks for Early, Late and Prompt replicas for I and Q components with respect to Frequency

The code phase DLL affects the two important parameters – code loop thermal noise error and maximum LOS dynamic threshold. Usually, the DLL discriminators are normalized so that, there is no amplitude sensitivity. Hence, under rapidly changing Signal-to-noise-ratio (SNR), DLL tracking is independent of the Automatic Gain Controller (AGC).

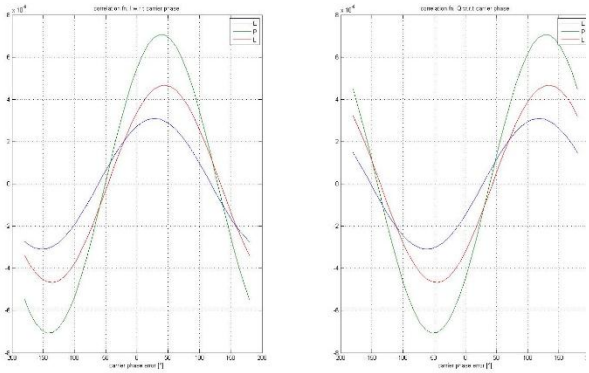

Figure 21. Correlation peaks for Early, Late and Prompt replicas for I and Q components with respect to carrier phase

From figure 22, it can be verified that the Early minus Late power discriminator has similar error characteristics as that of the Early minus Late envelope. Furthermore, these two discriminators have most linearity for the $\pm\frac{1}{2}$ chip range. On the other hand, the quasi-coherent and the dot-product discriminators have non-linear characteristics. But it is down to the fact that the receiver signal itself is not in PLL (simulated). And these two discriminators need the carrier to be in PLL. This is also ascertained by the fact that the Q components in the correlation still has significant value and that the I-component is not a constant value. This can also be verified in figure 23.a, where the non-coherent Early minus Late envelope DLL is linear over the full chip range over a wide range of Doppler frequencies. However, in figure 23.b, the coherent discriminator merely shows linearity for 0-doppler but tends towards highly non-linear behavior as the Doppler-frequencies are changed. It is well known that the coherent discriminator is

a better choice for a GPS receiver but it is important that the carrier be in PLL before the discriminator is employed.

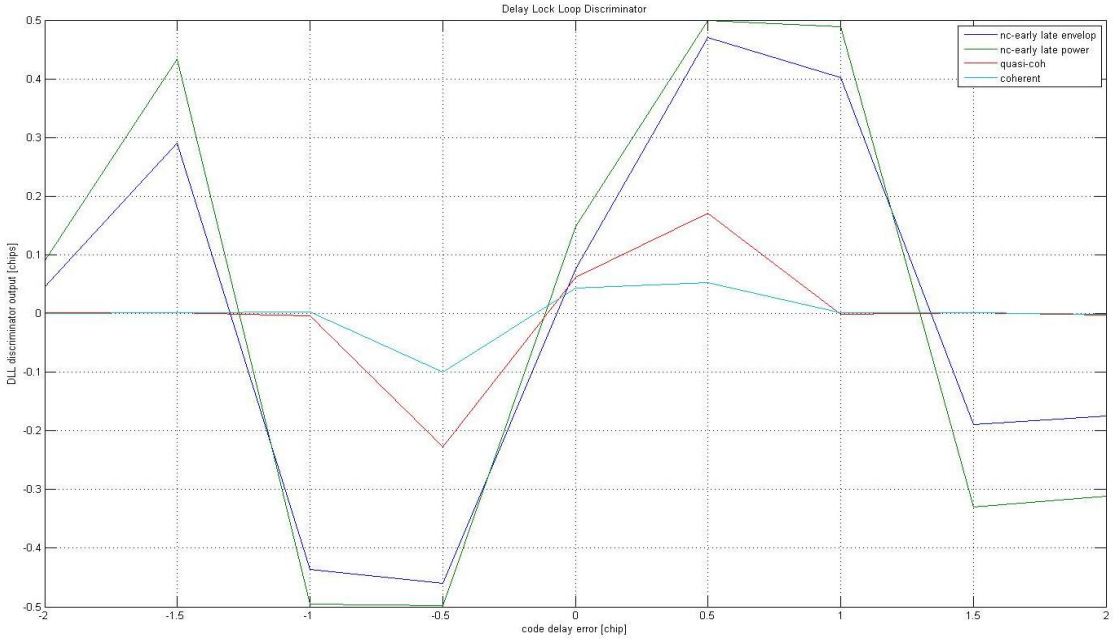

Figure 22. Discriminator S-curves for non-coherent-early late overlap (blue), non-coherent-early late power (green), quasi-coherent (red) and coherent (cyan)

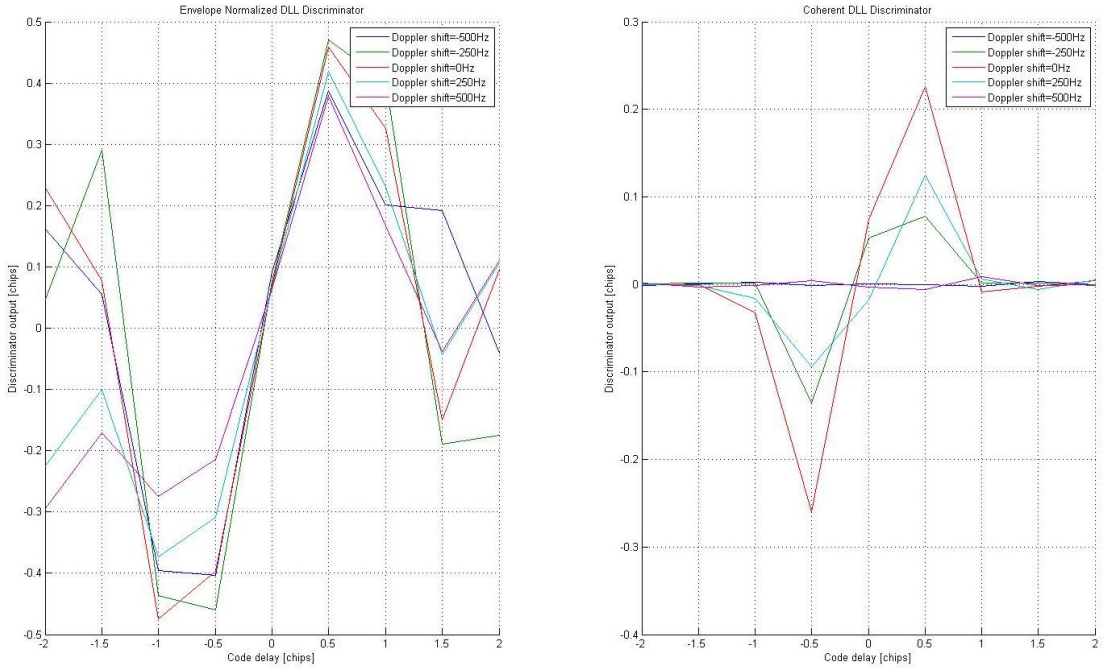

Figure 23. Discriminator S-curves for a)non-coherent-early late envelope and b)Coherent DLL at different Doppler Frequencies

The following discriminators were employed as shown in Table: 4.

Table: 4	
Non-coherent Early Minus Late envelope	$\frac{1}{2}\frac{E-L}{E+L}$ where, $E = \sqrt{{I_E}^2 + {Q_E}^2}$ and $L = \sqrt{{I_L}^2 + {Q_L}^2}$
Non-coherent Early Minus Late power	$\frac{1}{2}\frac{(E^2 - L^2)}{(E^2 + L^2)}$
Quasi-coherent dot product power	$\frac{1}{2}\frac{[(I_E - I_L).I_P + (Q_E - Q_L).Q_P]}{I_{P(max)}}$
Coherent dot product	$\frac{1}{2}\frac{(I_E - I_L).I_P}{I_{P(max)}}$

PLLs are employed in order to track the carrier phase of incoming GNSS signal by providing the correction in phase as an output. It tracks the current misalignment between the Prompt correlator's carrier replica and the incoming signal phase.

$$I_P = AdR_x(\tau_e)\cos(\varphi_e) \quad \text{(ix)}$$

$$Q_P = -AdR_x(\tau_e)\sin(\varphi_e) \quad \text{(x)}$$

Where, P: Prompt replica.

The philosophy of PLL is that in a completely phase locked receiver, the in-phase component will have maximum amplitude while the quadrature component will be the minimum. By determining both components, the carrier phase error can be determined using different discriminators.

The major problem of the conventional PLL is data-bit transition since I and Q components reverse their signs; which reduces the discriminator output. Also, since, they track all four quadrants, they have a 6-dB improvement over Costas loops for dataless carrier tracking. Costas loops are fundamentally insensitive to data-bit transitions. Contrary to conventional PLLs, Costas loops track over two quadrants. But in presence of noise, both types of PLLs are linear only near 0 region.

In Figure 24, it can be seen that the PLLs are centered about $\pi/4$. The conventional PLL (atan2) shows a full $\pm\pi$ range while the other Costas loops show only a $\pm\pi/2$ range. Also, apart from the tangent functions, the other functions are all non-linear in nature.

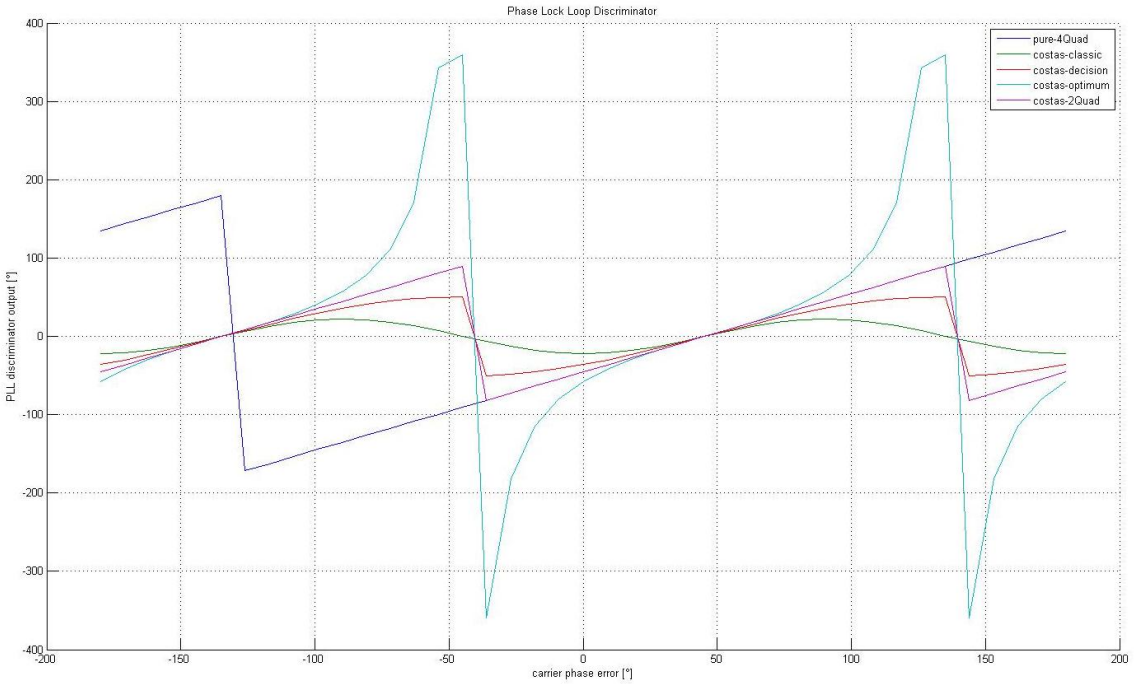

Figure 24. Discriminator Conventional [atan2] (blue), Classic (green), Decision (red) and Sub-optimal (cyan), Costas-atan(magenta)

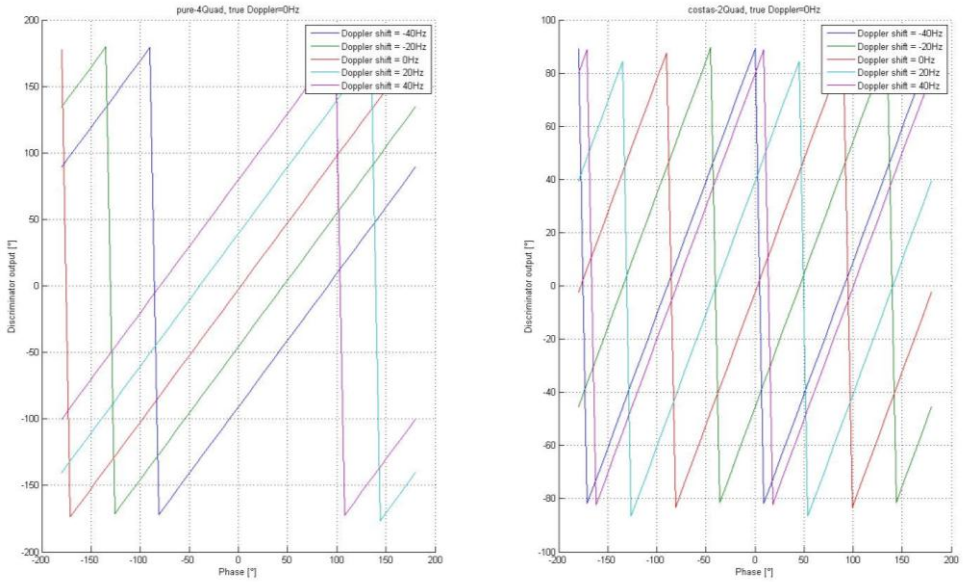

Figure 25. a)Conventional 4-quad b)Costas 2-quad tangent functions for different frequencies

In Figure 25, it is observed that for the Doppler frequencies, the curves shift accordingly to signify the phase error in carrier. And although it appears that the 4-quad conventional PLL is having a greater range, it suffers from bit-transition problems. Given a known initial carrier phase, the Doppler frequencies can be estimated from the carrier phase change. The discriminators employed are listen in Table: 5.

Table: 5	
Four quadrant arctangent	$ATAN2(Q_P, I_P)$
Costas two quadrant arctangent	$ATAN(Q_P, I_P)$
Costas Classic analog	$Q_P \times I_P$
Costas Decision directed	$Q_P \times Sign(I_P)$
Costas suboptimal	Q_P / I_P

FLLs achieve carrier tracking (carrier wipeoff) by generating the appropriate frequency and allowing the phase to change according to the SV signal. When data-bit transitions are unknown, it is easier to operate FLL and get a lock-state since FLLs are less vulnerable to bit-transitions.

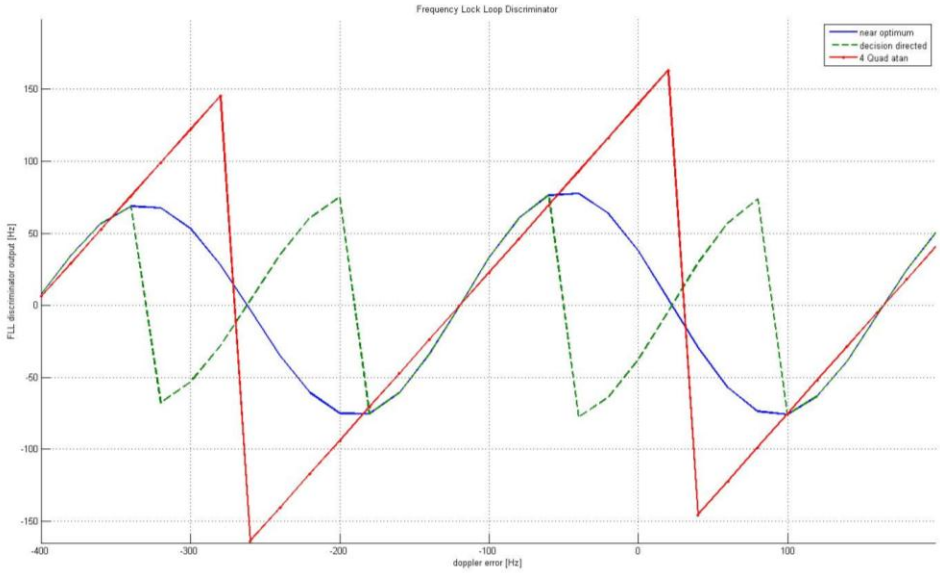

Figure 26. FLL discriminators: 4-quad (red), optimal (blue), decision-directed (green)

From figure 26, it can be observed that the Frequency pull-in range of the FLL is 333.33Hz since the predetection time is 3ms. Also, the 4-quadrant atan2 and the cross-optimal discriminator have a one-sided pull-in range are half the predetection bandwidths. Furthermore, the decision-directed discriminator has pull-in range of quarter that amount.

For this purpose, the following the discriminators were used as shown in Table: 6

Table: 6	
Four quadrant arctangent	$ATAN2(dot, cross)/(t_2 - t_1)$, where $dot = I_{P1} \times I_{P2} + Q_{P1} \times Q_{P2}$, and $\text{cross} = I_{P1} \times Q_{P2} - I_{P2} \times Q_{P1}$
Optimal	$\text{cross}/(t_2 - t_1)$
Decision-directed	$\text{cross} \times \text{sign}(\text{dot})/(t_2 - t_1)$

The performance of the discriminators is subject to the errors due to the thermal noise code jitter and dynamic stress error. Using carrier-aiding, that is, using the carrier measurement as a feedforward into the DLL, the dynamic stress error is significantly reduced (only in case of code phase tracking). As discussed before, the normalized discriminators that are employed have no amplitude sensitivity. Hence, the DLL performance is independent of the AGC parameters. However, a reduction in SNR will result in reduction of the slope of the discriminator outputs. Also, since bandwidth is directly proportional loop gain, under low SNR conditions, the loop bandwidth reduces thereby resulting in poor dynamic stress response. (Since dynamic stress response is dependent on loop bandwidth).

Table: 7 (Performance of Tracking loops)	
DLL	$\sigma_{th} = \frac{1}{T_c}\sqrt{\frac{B_n \int_{-B_{fe}/2}^{B_{fe}/2} S_s(f)sin^2(\pi f \delta T_c)df}{(2\pi)^2 C/N_0[\int_{-B_{fe}/2}^{B_{fe}/2} f S_s(f)sin(\pi f \delta T_c)df]^2}} \times \sqrt{1 + \frac{\int_{-B_{fe}/2}^{B_{fe}/2} S_s(f)cos^2(\pi f \delta T_c)df}{TC/N_0[\int_{-B_{fe}/2}^{B_{fe}/2} S_s(f)cos(\pi f \delta T_c)df]^2}}$ (non-coherent)
PLL	$\sigma_{th} = \frac{\lambda}{2\pi}\sqrt{\frac{B_n}{C/N_0}(1 + \frac{1}{2TC/N_0})}$ (arctangent)
FLL	$\sigma_{th} = \frac{\lambda}{2\pi T}\sqrt{\frac{4FB_n}{C/N_0}(1 + \frac{1}{TC/N_0})}$

Based on Table: 7, it can be inferred that a low SNR value will cause a higher variance of the loop errors.

VII. Filter loop design (PLL)

Parameters of design:

i. **Line-of-sight dynamic jerk stress** = $5\ g/sec$
ii. **Receiver is unaided**
iii. **The receiver must maintain PLL**

In order to surmount the LOS dynamic jerk stress, a *third order filter* is designed.

$$\dddot{\theta} = 9.81\ {}^{m}/_{sec^2} \times \frac{2\pi}{0.1903}\ {}^{rad}/_{m} \times 5\frac{g}{sec} \approx 1620\ {}^{rad}/_{sec} \quad \text{(xi)}$$

$$Bandwidth.\ B_n \geq \frac{1}{1.2}\sqrt[3]{\frac{\dddot{\theta}}{0.2}} = 16.75\ Hz \quad \text{(xii)}$$

Since, the Bandwidth, B_n, is less than 18 Hz, the design is stable.

Figure 27 shows the variation of Bandwidth with respect to the radial jerk acceleration. The maximum Bandwidth required is 16.75 and hence it does not suffer from conditional oscillatory behavior.

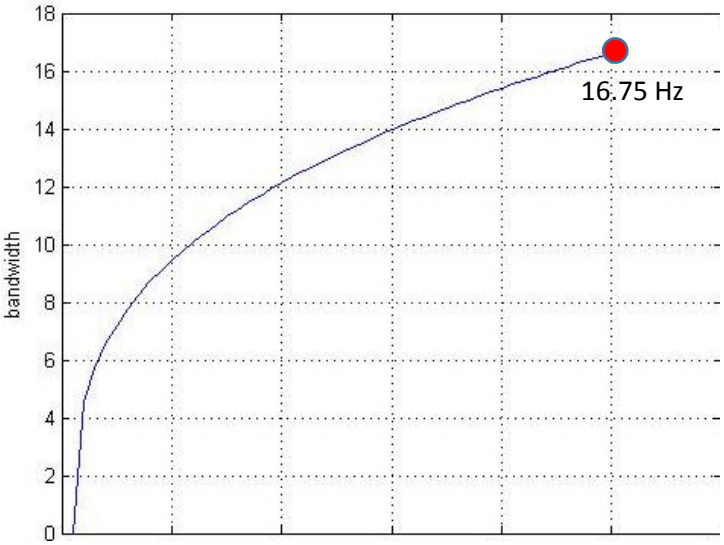

Figure 27. Bandwidth curve for the filter design

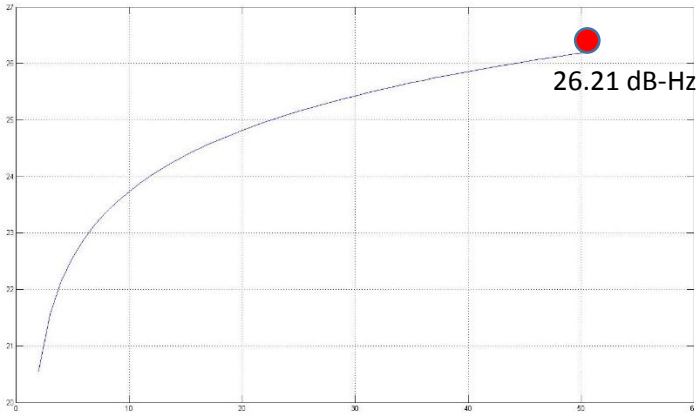

gure 28. $\frac{C}{N_0}$ curve for the filter design

Based on Figures 27 and 28, it can be concluded that the loop Bandwidth needs to be greater than 16.75 Hz while the $\frac{C}{N_0}$ should be at least 26.21 dB-Hz for the jerk-stress to be gracefully handled.

Figure 29 demonstrates the thermal jitter curves for different Bandwidth values. For a nominal bandwidth of 1 Hz and a $\frac{C}{N_0}$ of 25, we get a thermal jitter variance, ${\sigma_{t,PLL}}^2$ of 5.1764 degrees.

The vibration-induced oscillator phase noise variance, ${\sigma_v}^2$, is found out to be 1.353 degrees under the assumption that the vibrational power is flat within [20, 200] Hz range and a sensitivity of 0.005 $\frac{g}{sec^2}$.

In Figure 30, the Allan deviation characteristics are plotted for the L1-carrier with an Allan variance of 1×10^{-10} for the oscillator itself. The contribution to the PLL error variance, ${\sigma_a}^2$, was found to be 1.5 degrees for a nominal bandwidth of 16.75 which is the least requirement for dealing with the jerk stress specified in the problem.

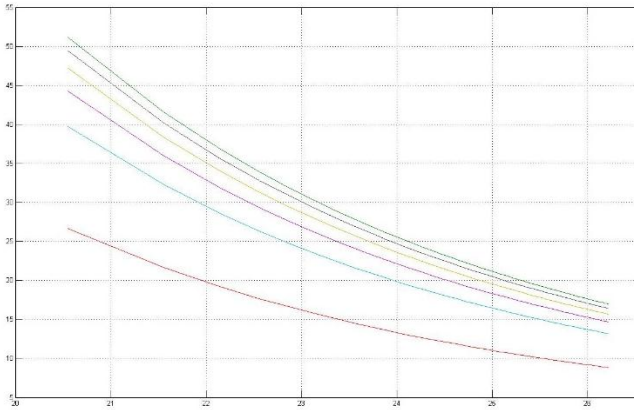

Figure 29. Thermal jitter curves for different bandwidths

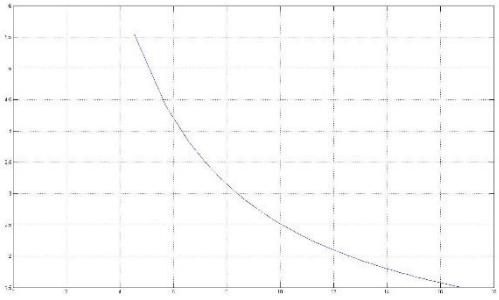

Figure 30. Allan variance oscillator phase curves for bandwidths

And furthermore, the dynamic stress error was computed as follows:

$$\theta_e = 0.4827 \times \frac{{d^3R}/{dt^3}}{B^3} \quad \text{(xiii)}$$

Since R has to be mentioned in terms of degrees, the given jerk value is converted accordingly by using the carrier frequency and θ_e was found to be, 9.52 degrees for a nominal bandwidth of 16.75 Hz.

The total PLL variance is known to be,

$$(\text{PLL})\sigma_{PLL} = \sqrt{{\sigma_{t,PLL}}^2 + {\sigma_v}^2 + {\sigma_a}^2} + {\theta_e}/{3} = 6\ degrees \quad \text{(xiv)}$$

Hence, the variance $(\text{PLL})\sigma_{PLL}$ was found to be within the limit of 15 degree as is suggested.

Based on these computations, a nominal Bandwidth of 16.75 Hz is decided upon. Hence,

$$\omega_{0,PLL} = 1.2B_{PLL} = 20\ rad/sec \quad \text{(xv)}$$

$$a_3 = 1.1;\ b_3 = 2.4 \quad [1]$$

Based on these parameters, the following filter was designed,

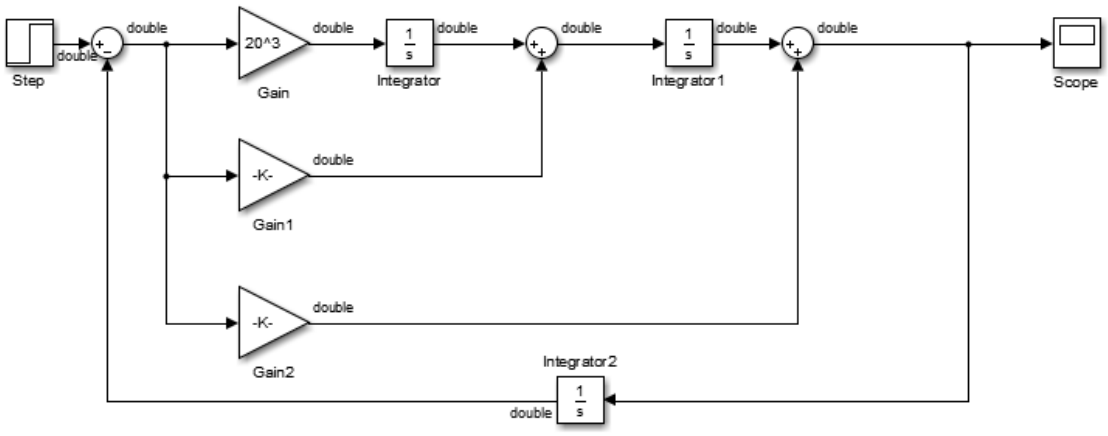

Figure 31. Third-order PLL filter based on design parameters

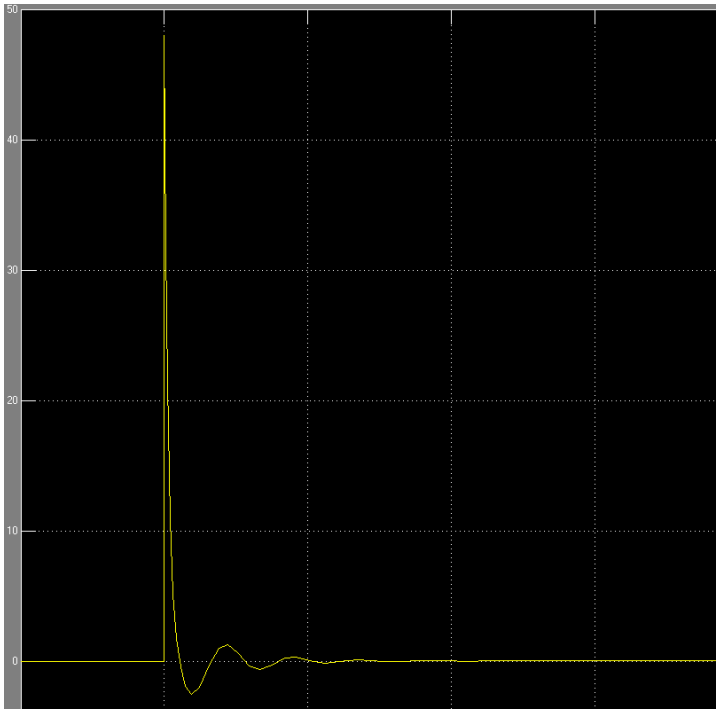

Figure 32. Unit-step response of the filter design

The filter was tested for a unit-step response and Figure 32, shows the output on the scope of the Simulink simulation.

VIII. References

[1] Dr.-Ing. Ayse Sicramaz Ayaz, "*Signal Tracking*": Lecture notes and presentation at ESPACE-2015.

[2] Elliot D. Kaplan, "Understanding GPS – Principles and applications": Satellite Signal Acquisition, Tracking, and Data Demodulation.

[3] Frendrick Johansson, 1998, *GPS Satellite Signal Acquisition and Tracking*, the report.

[4] Rishija Misra, and Shubham Palod, *Code and Carrier Tracking Loops for GPS C/A Code*, IJPAST.

[5] Abdehalim Zekry, *Implementation of a Complete GPS Receiver on the C6713 DSP through Simulink Receiver*, Journal of Global Positioning Systems.